

Showcasing research from the Energy Laboratory,  
Samsung Advanced Institute of Technology, Republic of Korea.

Title: Operating mechanisms of electrolytes in magnesium ion batteries: chemical equilibrium, magnesium deposition, and electrolyte oxidation

Operating mechanisms of Mg electrolytes are clarified by studying the characteristics of Mg complexes, solvation, chemical equilibrium, Mg-deposition processes, electrolyte-oxidation processes, and oxidative degradation mechanism of RMgCl-based electrolytes, using *ab initio* calculations. This article first provides a methodological scheme for calculating Mg reduction potential values in non-aqueous electrolytes and electrochemical windows, and also describes a strategy for designing Mg electrolytes to maximize the electrochemical windows and oxidative stabilities.

### As featured in:



See Dong Young Kim,  
Seok-Soo Lee et al.,  
*Phys. Chem. Chem. Phys.*,  
2014, **16**, 25789.

# Operating mechanisms of electrolytes in magnesium ion batteries: chemical equilibrium, magnesium deposition, and electrolyte oxidation<sup>†</sup>

Cite this: *Phys. Chem. Chem. Phys.*, 2014, 16, 25789

Dong Young Kim,<sup>\*a</sup> Younhee Lim,<sup>a</sup> Basab Roy,<sup>a</sup> Young-Gyo Ryu<sup>b</sup> and Seok-Soo Lee<sup>\*a</sup>

Since the early nineties there have been a number of reports on the experimental development of Mg electrolytes based on organo/amide-magnesium chlorides and their transmetalations. However, there are no theoretical papers describing the underlying operating mechanisms of Mg electrolytes, and there is no clear understanding of these mechanisms. We have therefore attempted to clarify the operating mechanisms of Mg electrolytes by studying the characteristics of Mg complexes, solvation, chemical equilibrium, Mg-deposition processes, electrolyte-oxidation processes, and oxidative degradation mechanism of RMgCl-based electrolytes, using *ab initio* calculations. The formation and solvation energies of Mg complexes highly depend on the characteristics of R groups. Thus, changes in R groups of RMgCl lead to changes in the equilibrium position and the electrochemical reduction and oxidation pathways and energies. We first provide a methodological scheme for calculating Mg reduction potential values in non-aqueous electrolytes and electrochemical windows. We also describe a strategy for designing Mg electrolytes to maximize the electrochemical windows and oxidative stabilities. These results will be useful not only for designing improved Mg electrolytes, but also for developing new electrolytes in the future.

Received 24th March 2014,  
Accepted 2nd May 2014

DOI: 10.1039/c4cp01259c

[www.rsc.org/pccp](http://www.rsc.org/pccp)

## 1. Introduction

There is much scientific interest in developing new energy-storage systems,<sup>1,2</sup> and metallic Mg has many promising properties as an anode material.<sup>3–5</sup> Mg ions carry two electrons per atom, so they are potentially more efficient energy-storage systems, compared to Li ions. Mg is relatively abundant, cheap, safe, lightweight, and environmentally friendly. Moreover, Mg deposition does not lead to dendrite formation,<sup>6</sup> which renders Li metal unsafe for utilization as an anode material.

However, the development of Mg batteries is technically challenging, because of the difficulties caused by the migration of bivalent Mg ions at solid-electrolyte interfaces and in solid phases. In contrast to Li-battery systems,<sup>7</sup> Mg electrodes can therefore only behave reversibly under passivation-free conditions.<sup>3</sup> This situation requires the electrolytes of Mg

batteries to be inert to the battery components, but Mg metal reacts with a variety of aprotic solvents (*e.g.*, carbonates, esters, and acetonitrile) and commonly used anions (*e.g.*, ClO<sub>4</sub><sup>−</sup>, AsF<sub>6</sub><sup>−</sup>, PF<sub>6</sub><sup>−</sup>, and BF<sub>4</sub><sup>−</sup>), resulting in the formation of blocking surfaces.<sup>8</sup>

Since the early 1990s, it has been known that certain ethereal Grignard reagents (organomagnesium halides) are electrically conductive, with reversible Mg deposition/dissolution satisfying the passivation-free conditions.<sup>9–11</sup> However, Grignard reagents are usually strong reducing agents with insufficient anodic stability. The width of the electrochemical window of ethyl/phenylmagnesium chloride is ~1.0/2.0 V.<sup>12</sup> Compared with organomagnesium compounds, amide-magnesium halides, which are also called Hauser bases, generally have higher oxidative stabilities, because of the higher electronegativity of nitrogen. On this basis, Lobitz *et al.* suggested the use of hexamethyldisilazide magnesium chloride (HMDSMgCl), where the electron-rich Si–N–Si core stabilizes the HMDS anion. However, the width of the electrochemical window of HMDSMgCl is only ~2.0 V.<sup>13</sup>

In 1990, Gregory *et al.*<sup>12</sup> proposed Mg battery electrolytes containing aluminate- and boron-based salts to improve the anodic stability and ionic conductivity. Aurbach *et al.*<sup>14–18</sup> expanded Gregory's work. They developed several electrolytes based on Mg-organoaluminate salts, in which R<sub>m</sub>MgCl<sub>2–m</sub> Lewis bases

<sup>a</sup> Energy Storage Laboratory, Samsung Advanced Institute of Technology, Samsung Electronics, 130 Samsung-ro, Suwon, Gyeonggi-do 443-803, Republic of Korea. E-mail: dy777.kim@samsung.com, seoksoo.lee@samsung.com

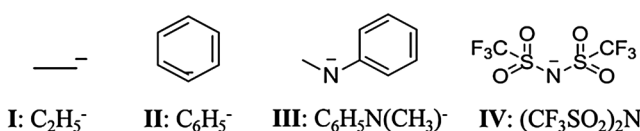
<sup>b</sup> Advanced Materials Laboratory, Samsung Advanced Institute of Technology (SAIT-America), 1 Cambridge Center, Cambridge, MA 02421, USA

<sup>†</sup> Electronic supplementary information (ESI) available: SI-1: tables of energy values in Fig. 2; SI-2: tables of energy and equilibrium constant values in Fig. 3; SI-3: tables of energy values in Fig. 7; SI-4 and 5: calculated reaction pathways; and SI-6: calculation methods. See DOI: 10.1039/c4cp01259c

and  $\text{AlR}_n\text{Cl}_{3-n}$  Lewis acids react by transmetalation of R groups from Mg to Al. An all-phenyl-complex electrolyte, formed from the reaction of  $\text{PhMgCl}$  with  $\text{AlCl}_3$  in a 2:1 ratio in tetrahydrofuran (THF), shows a high oxidative stability of  $\sim 3.2$  V *versus* Mg, with 100% cycling efficiency.<sup>19</sup> Muldoon *et al.* developed a crystallized electrolyte, formed from the reaction of  $\text{HMDSMgCl}$  with  $\text{AlCl}_3$  in a 3:1 ratio, with an oxidative stability of  $\sim 3.2$  V *versus* Mg and 100% cycling efficiency.<sup>20</sup> However, the  $\text{Cl}^-$  ions in the electrolyte corrode non-noble-metal electrodes; this further justifies attempts to develop non-corrosive Mg electrolytes.<sup>21,22</sup> We also note that there have been endeavors to develop Mg-ion insertion-type anode materials for use as conventional battery electrolytes,<sup>23–27</sup> which would be beyond the scope of this study.

Although a number of experimental studies of electrolytes based on organo/amide-magnesium chlorides ( $\text{RMgCl}$ ) and their transmetalations have been reported, there are no theoretical papers on the underlying operation and degradation mechanisms of Mg electrolytes, and there is no clear understanding of these mechanisms. To improve the operating properties of electrolytes, such as oxidative, reductive, air, and corrosion stabilities, conductivity, and reversibility, it is vital to understand the underlying electrolyte mechanism. It is therefore important to clarify the operating mechanisms of electrolytes based on  $\text{RMgCl}$ . This study is the first to elucidate the mechanistic details.

We tried to gain a deep understanding of the general rules and trends regarding (i) chemical equilibrium, with prediction of the dominant cations, anions, and neutral species, and (ii) the Mg-deposition mechanism, with a suggested methodological scheme for calculating Mg reduction potentials in non-aqueous electrolytes. We also investigated (iii) electrolyte oxidation and oxidative degradation, with evaluation of the electrochemical windows of  $\text{RMgCl}$ -based electrolytes using “model chemistry” based on *ab initio* calculations.<sup>28–32</sup> Two organic and two amide anions, **I–IV**,<sup>12,33,34</sup> with different ionization energies were considered.



The first ionization energies ( $\text{IE}_1$ ) increase in the order **I** < **II** < **III** < **IV**. The  $\text{IE}_1$  values of **I**, **II**, **III**, and **IV** in THF at 298 K are 2.15, 3.79, 3.80, and 7.17 eV, respectively, at the CCSD(T)/aug-cc-pVDZ level;<sup>35,36</sup> the  $\text{IE}_1$  of  $\text{Cl}^-$  in THF at 298 K is 6.03 eV at the same level of theory (calculation details are provided in the ESI†). The  $\text{IE}_1$  values of **II** and **III** are almost equivalent, but **III** has more steric hindrance. (iv) Based on our understanding, we also discuss the recent developments in Mg electrolytes and a strategy for designing electrolytes for Mg batteries to maximize the reductive and oxidative stabilities and the electrochemical window. In both fundamental and applied points of view, this study provides important information on the development of Mg electrolytes and batteries.

## 2. Equilibrium aspects

The equilibrium of ethereal  $\text{RMgCl}$  is complex. The equilibrium species are a mixture of various combinations of compounds, characterized by their  $\text{R}/\text{Cl}^-$  ratios. The neutral equilibrium is  $2\text{RMgCl} \leftrightarrow \text{R}_2\text{Mg} + \text{MgCl}_2$ , and is known as the Schlenk equilibrium. Aggregated conformations,  $n\text{RMgCl} \leftrightarrow (\text{RMgCl})_n$ ,  $n > 2$ , can exist, but usually at high concentrations. Ionic species, namely  $\text{R}/\text{Cl}^-$  and  $[\text{R}_n\text{MgCl}_m]^-$  ( $n + m = 3$ ,  $n = 0, 1, 2, 3$ ) anions, and  $[\text{RMg}]^+$  and  $[\text{MgCl}]^+$  cations, can be formed (Fig. 1). Although the characteristics of R determine the equilibrium positions of  $\text{RMgCl}$  in THF, the chemical equilibrium also depends on the concentration and temperature.<sup>37</sup>

As the first ionization energy of R increases, the covalent character of the Mg-R bond in  $\text{MgR}^+$  decreases; therefore, the strength of the Mg-R bond decreases and the bond becomes unstable. The gas-phase interaction free energies between  $\text{Mg}^{2+}$  and R in **I**, **II**, **III**, and **IV** are  $-19.60$ ,  $-16.06$ ,  $-15.51$ , and  $-13.87$  eV, respectively ( $\Delta\Delta G_{\text{int}}$ ,  $n = 1$  in Fig. 2a). The solvation effects depend on the characteristics of the Mg complex as well as the characteristics of the solvent itself – the strength of the Mg-R bond in the Mg complex determines the interaction

<b>RMgCl</b>		
Anions:	Neutrals:	Cations:
<b>R</b> <sup>-</sup>	<b>RMgCl</b>	<b>RMg</b> <sup>+</sup>
<b>R</b> <sub>3</sub> <b>Mg</b> <sup>-</sup>	<b>MgCl</b> <sub>2</sub>	<b>MgCl</b> <sup>+</sup>
<b>R</b> <sub>2</sub> <b>MgCl</b> <sup>-</sup>	<b>R</b> <sub>2</sub> <b>Mg</b>	
<b>RMgCl</b> <sub>2</sub> <sup>-</sup>		
<b>MgCl</b> <sub>3</sub> <sup>-</sup>		
<b>Cl</b> <sup>-</sup>	Aggregated forms	

Fig. 1 Possible ionic and neutral species obtained from  $\text{RMgCl}$  in solution.

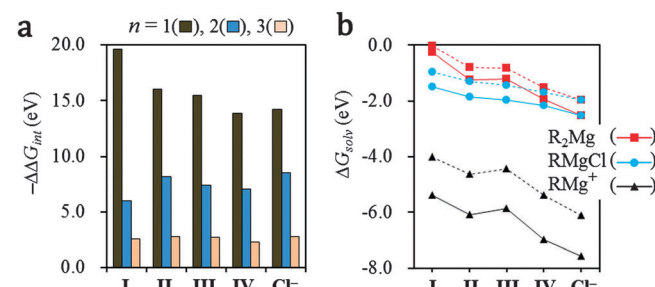
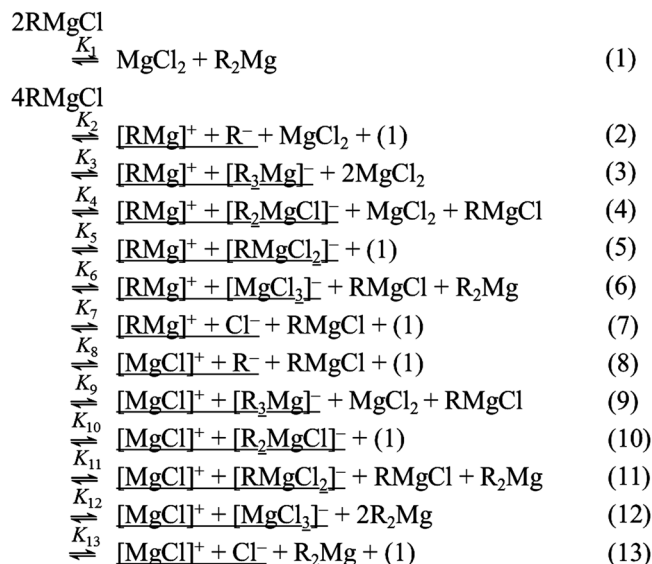


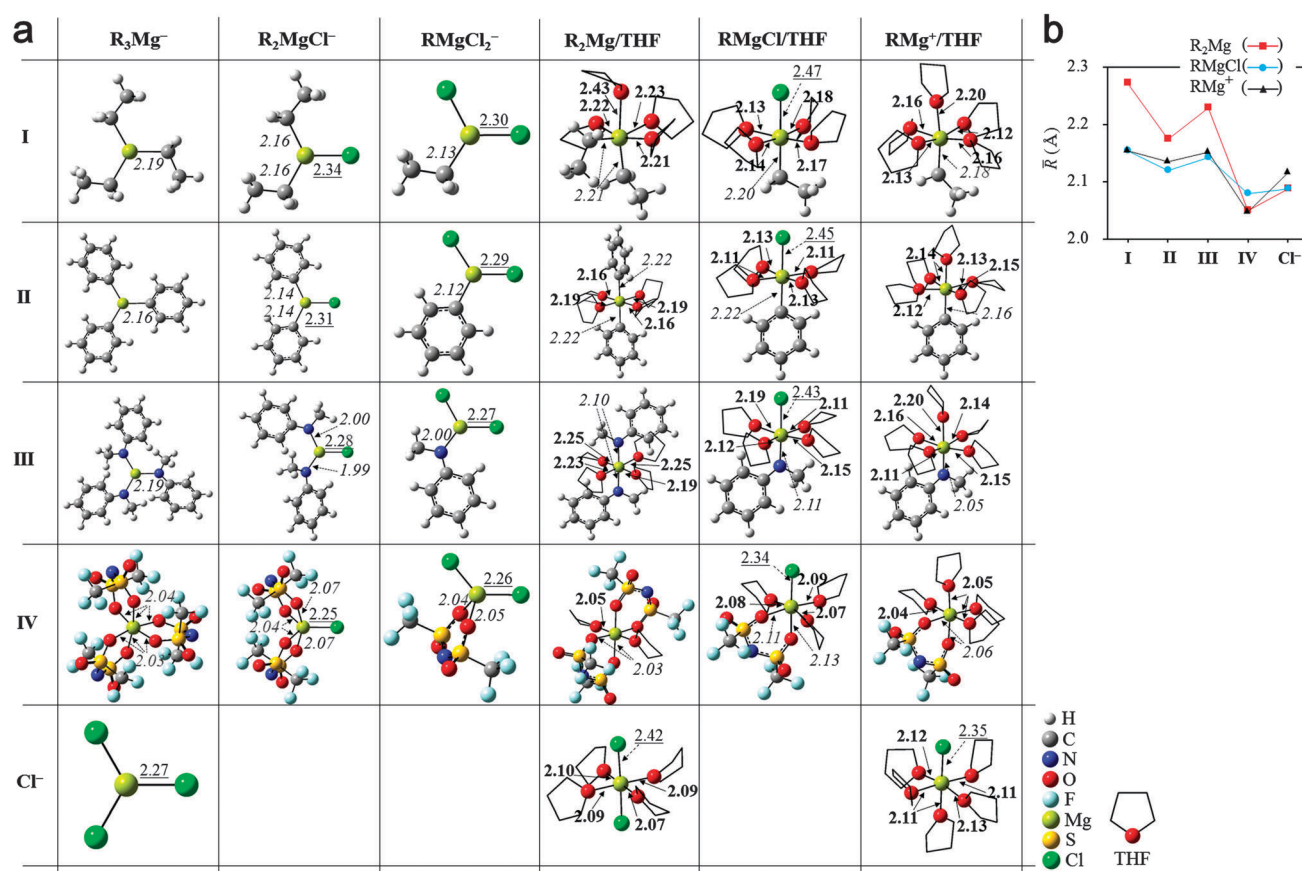
Fig. 2 (a) Gas-phase successive interaction free energies [ $\Delta\Delta G_{\text{int}} = G(\text{R}_n\text{Mg}) - G(\text{R}_{n-1}\text{Mg}) - G(\text{R})$ ] of Mg complexes formed by sequential addition of R groups from  $n = 1$  to  $n = 3$  at the M062X/6-311+G\*\* level.<sup>35,38</sup> (b) solvent-coordination free energies [dotted lines,  $\Delta G_{\text{coor}} = G_g(n\text{THFA}) - nG_g(\text{THF}) - G_g(\text{A})$ , where A represents Mg complexes,  $n\text{THFA}$  represents THF-coordinated A, and  $G_g(\text{A})$  and  $G_g(n\text{THFA})$  are the gas-phase free energies of the complexes of A and  $n\text{THFA}$ , respectively] and solvation free energies [ $\Delta G_{\text{solv}} = \Delta G_{\text{coor}} + \Delta G_{\text{solv}}(n\text{THFA})$ ] of  $\text{R}_2\text{Mg}$ ,  $\text{RMgCl}$ , and  $\text{RMg}^+$  at the M062X/6-311+G\*\* level. Tables of energy values are provided in the ESI† (SI-1). Optimized geometries of THF-coordinated  $\text{R}_2\text{Mg}$ ,  $\text{RMgCl}$ , and  $\text{RMg}^+$  are presented in Fig. 4.

Fig. 3 Possible chemical reactions of  $4RMgCl$ ; ionic species are underlined.

strength between the Mg complexes and solvent molecules; the molecular structures of the solvent and R both affect solvation sterically. In Fig. 2b, the solvation free energies ( $\Delta G_{\text{solv}}$ ) and

coordination free energies ( $\Delta G_{\text{coord}}$ ) of neutral ( $R_2Mg$ ,  $MgCl_2$ , and  $RMgCl$ ) and cationic ( $RMg^+$  and  $MgCl^+$ ) species are plotted for different R groups. To calculate  $\Delta G_{\text{coord}}$ , the remaining sites on each Mg center for all the neutral and cationic Mg species are coordinated through the O atoms of THF molecules, maintaining a coordination number of six (Fig. 4). An implicit solvent is then applied to the THF-coordinated Mg complexes, and  $\Delta G_{\text{solv}}$  is evaluated. As the strength of the Mg-R bond decreases, the solvent stabilization of the Mg complexes increases in the order **I** < **II** < **IV**. Although the IE<sub>1</sub> values of **II** and **III** are almost equivalent, the  $\Delta G_{\text{solv}}/\Delta G_{\text{coord}}$  value for  $MgR^+$  with **III** is slightly higher than that with **II**, because of steric hindrance by **III**. In the case of **IV**, the Mg-R complexes are characterized by bidentate structures through the two O atoms of each  $SO_2$  group, and this blocks solvent coordination. Thus, although the IE<sub>1</sub> of  $Cl^-$  (6.03 eV) is less than that of **IV** (7.17 eV), the solvent stabilization of Mg complexes involving  $Cl^-$  is greater than that of those involving **IV**.

To consider not only neutral equilibrium but also ionic equilibrium, we investigated the energy profiles of the relative stabilities of  $4RMgCl$  and the possible combinations of neutral and ionic species, except aggregated forms (eqn (1)–(13), Fig. 3). Eqn (1) is the Schlenk equilibrium, eqn (2)–(7) include an  $[RMg]^+$  cation, and eqn (8)–(13) include an  $[MgCl]^+$  cation. The free energy profiles of eqn (1)–(13), based on  $4RMgCl$  in the gas phase, are

Fig. 4 (a) Optimized structures of  $R_3Mg^-$ ,  $R_2MgCl^-$ ,  $RMgCl_2^-$ ,  $R_2Mg$ ,  $RMgCl$ , and  $RMg^+$  at the M062X/6-311+G\*\* level. Neutral and cationic Mg complexes are six coordinated by THF molecules and R groups. Bond distances between Mg and Cl, THF, and R are denoted grey/underlined, grey/italic, and black/bold characters, respectively. (b) Average bond distances between the O atoms of THF molecules and the Mg centers of  $R_2Mg$ ,  $RMgCl$ , and  $RMg^+$ .

presented in Fig. 5a. To investigate the solvent-coordination effects of THF molecules on Mg complexes, the  $\Delta G_{\text{coord}}$ -corrected energy profiles are plotted in Fig. 5b; the free energy profiles in THF are presented in Fig. 5c. The equilibrium constants ( $K$ ) at 298 K, calculated from the equation  $\Delta G = -RT \ln K$ , where  $\Delta G$  is the relative energy in THF,  $R$  is the universal gas constant, and  $T$  is temperature, are shown in Fig. 5d.

The dominant neutral species in the Schlenk equilibrium is  $\text{RMgCl}$ , with a covalent R-Mg bond. The dominance of  $\text{R}_2\text{Mg} + \text{MgCl}_2$  (eqn (1)) increases with the increasing ionic nature of the R-Mg bond, and  $\text{R}_2\text{Mg} + \text{MgCl}_2$  becomes the dominant neutral species for **IV** in THF. While  $\text{R}_2\text{Mg}$

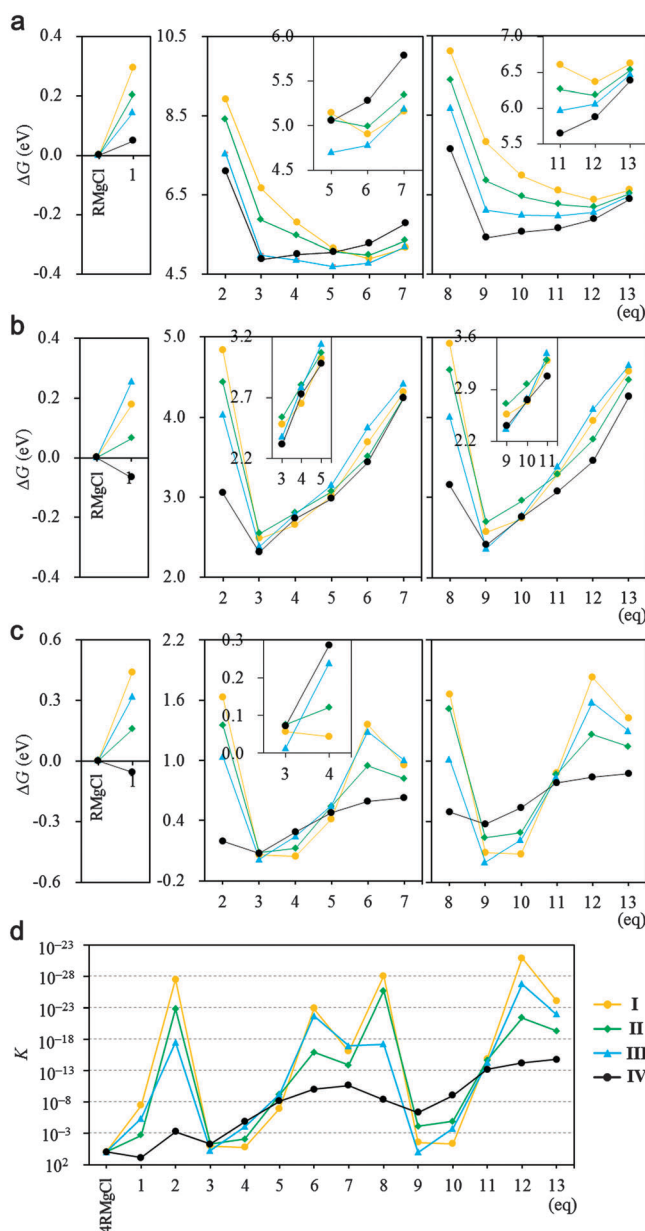


Fig. 5 Relative energy profiles for eqn (1)–(13) in the gas phase (a), in the THF-coordinated phase (b), and in the THF phase (c) at the M062X/6-311+G\*\* level. (d) Equilibrium constants for eqn (1)–(13) at 298 K. Tables of energy and equilibrium constant values are available in the ESI† (SI-2).

predominantly formed by the Schlenk equilibrium,<sup>37</sup>  $\text{MgCl}_2$  is predominantly formed by R-containing ionic species for **I–III**. In the gas phase, the neutral equilibrium in eqn (1) is more stable than the ionic equilibria in eqn (2)–(13) (Fig. 5a). In THF, however, the ionic eqn (3), (4), and (9) are more stable than eqn (1) for **I–III** (Fig. 5c). The ionic equations with the lowest energy states are eqn (4), (3), and (9) for **I**, **II**, and **III**, respectively. The relative energies of eqn (1) for **I**, **II**, and **III** are 0.44, 0.16, and 0.32 eV, respectively, and the relative energies of eqn (4) for **I**, eqn (3) for **II**, and eqn (9) for **III** are 0.04, 0.08, and 0.00 eV, respectively. Thus, although the dominant source of  $\text{R}_2\text{Mg}$  is the Schlenk equilibrium, the dominant source of  $\text{MgCl}_2$  is the formation of R-containing anionic/cationic species for **I–III**. The molar ratios  $[\text{MgCl}_2]/[\text{R}_2\text{Mg}] (\alpha)$  at 298 K are  $\sim 5.1 \times 10^6$ ,  $\sim 2.5 \times 10$ , and  $\sim 2.6 \times 10^5$  for **I**, **II**, and **III**, respectively, calculated from  $K_4/K_1$ ,  $K_3/K_1$ , and  $K_9/K_1$ , respectively (Fig. 5d). In the case of **IV**, eqn (1) ( $\text{MgCl}_2 + \text{R}_2\text{Mg}$ ) is the most stable equation; the dominant source of both  $\text{MgCl}_2$  and  $\text{R}_2\text{Mg}$  is the Schlenk equilibrium, and  $\alpha = \sim 1.0$ .

Although the dominant cation is  $[\text{MgR}]^+$ , with an ionic R-Mg bond (**IV**), the dominance of  $[\text{MgCl}]^+$  increases with increasing covalent character of the R-Mg bond. The gas-phase reaction free energies for



obtained by combining equations in Fig. 3, decrease with increasing  $\text{IE}_1$  values of the R groups; the energy values are 2.63, 2.17, 2.41, and 1.13 eV for **I**, **II**, **III**, and **IV**, respectively. As the  $\text{IE}_1$  of R increases, the interaction strength of the Mg-R bond decreases (Fig. 2a). However, because the solvation effect is greater for cationic species (Fig. 2b), the reaction energies for eqn (14) in THF become very similar for **I–IV**. Steric hindrance by **III** destabilizes the solvation of  $[\text{MgR}]^+$ , resulting in a lower reaction energy for eqn (14). These reaction free energies in THF are 0.51, 0.49, 0.28, and 0.55 eV for **I**, **II**, **III**, and **IV**, respectively, showing that  $[\text{MgR}]^+ + \text{MgCl}_2$  are more dominant species than  $[\text{MgCl}]^+ + \text{R}_2\text{Mg}$ . The molar ratio  $[\text{MgCl}]^+/\text{MgR}]^+ (\beta)$  therefore depends on the square of the molar ratio  $\alpha; \beta/\alpha^{0.5}$  at 298 K =  $\sim 5.4 \times 10^{-5}$ ,  $\sim 7.1 \times 10^{-5}$ ,  $\sim 4.2 \times 10^{-3}$ , and  $\sim 2.3 \times 10^{-5}$  for **I**, **II**, **III**, and **IV**, respectively. While THF-solvation stabilization is highest for  $\text{MgCl}_2$ , the solvation stabilization of  $\text{R}_2\text{Mg}$  increases with the increasing  $\text{IE}_1$  value of R. In the case of **III**, steric hindrance destabilizes  $\text{R}_2\text{Mg}$  formation by preventing solvent coordination. Thus,  $\alpha$  is lowest for **IV**, and the value increases with increasing covalent character of the R-Mg bond. Based on  $\alpha$ ,  $\beta$  at 298 K =  $\sim 1.2 \times 10^{-1}$ ,  $\sim 3.5 \times 10^{-4}$ ,  $\sim 2.1$ , and  $\sim 2.3 \times 10^{-5}$  for **I**, **II**, **III**, and **IV**, respectively.

$[\text{R}_3\text{Mg}]^-$  and  $[\text{R}_2\text{MgCl}]^-$  are the dominant anionic complexes, and  $[\text{MgCl}_3]^-$  and monomeric anions of R and  $\text{Cl}^-$  rarely exist for **I–III**; however, the dominance of  $[\text{MgCl}_3]^-$  and monomeric anions of R and  $\text{Cl}^-$  increases in the case of **IV**, which has a higher  $\text{IE}_1$ . For **IV**, R also becomes a dominant anionic species. In the gas-phase calculation (Fig. 5a), eqn (6) is the most stable equation among eqn (2)–(13) for **I**, showing that  $[\text{MgCl}_3]^-$  is the dominant anionic species for **I**. However, as the ionic nature of the R-Mg bond increases, the position of the equilibrium moves; the number of R-containing anionic species increases, and they

become dominant, with the most stable ionic equation for **IV** being eqn (3). In the THF-coordinated phase (Fig. 5b),  $[R_3Mg]^-$  becomes the dominant anionic species for **I–IV**, because of the coordination-driven high stabilization of  $MgCl_2$ . As the IE<sub>1</sub> value of R increases, the U-shaped relationship between the energies and eqn (2)–(7)/(8)–(13) becomes flatter. In the THF phase (Fig. 5c), this trend becomes more distinct. Thus, although  $[R_3Mg]^-$  and  $[R_2MgCl]^-$  are both dominant anionic species, the probabilities of the presence of  $[MgCl_3]^-$  and monomeric anions of R and  $Cl^-$  increase for **IV**. The molar ratios  $R^-:[R_3Mg]^-:[R_2MgCl]^-:[RMgCl_2]^-:[MgCl_3]^-:Cl^- (\gamma)$  at 298 K are evaluated by a simple comparison of the equilibrium constants in Fig. 5d, giving  $\sim 10^{-27}:\sim 1:\sim 1:\sim 10^{-6}:\sim 10^{-22}:\sim 10^{-15}$  for **I**,  $\sim 10^{-22}:\sim 1:\sim 1:\sim 10^{-1}:\sim 10^{-8}:\sim 10^{-15}:\sim 10^{-13}$  for **II**,  $\sim 10^{-17}:\sim 1:\sim 10^{-4}:\sim 10^{-9}:\sim 10^{-22}:\sim 10^{-17}$  for **III**, and  $\sim 10^{-2}:\sim 1:\sim 10^{-4}:\sim 10^{-7}:\sim 10^{-9}:\sim 10^{-10}$  for **IV**, respectively.

### 3. Mg deposition

There are several possible Mg-deposition pathways for ethereal  $RMgCl$  in complex equilibria. Aurbach *et al.* proposed that electrochemical Mg deposition in ethereal  $RMgCl$  systems occurs *via* electron transfer to species such as  $RMg^+$  or  $MgCl^+$  adsorbed on the electrode surfaces.<sup>14,16</sup> The Mg-deposition process is influenced not only by adsorbed species but also by the microstructures of regions interacting with adsorbed species. Solvent-molecule-coordinated intermediate species,  $RMg_s$  or  $MgCl_s$ , on the Mg surface could be formed by an initial electron reduction process, followed by formation of a reduced Mg atom on the Mg metal surface by a second electron transfer to the intermediate species, with breaking of the R–Mg or Mg–Cl bond. Finally, a monomeric anion, R or  $Cl^-$ , would be formed in solution – Path 1 in Fig. 6. In the second electron reduction process, cationic/neutral Mg complexes near the first reduced intermediate,  $RMg_s$  or  $MgCl_s$ , can aid the reaction, producing energetically stable neutral/anionic Mg complexes in solution – Path 2/3 in Fig. 6.

The free energies for  $Mg/Mg^{2+}$  reduction of a Grignard reagent ( $\Delta G_{\text{red}}$ ) *via* Paths 1–3 are given by following equations

$$\Delta G_{\text{red}}^{\text{Path1}} = G_s(Mg) + G_{\text{THF}}(R1) - G_{\text{THF}}(MgR1^+) - 2\Phi_M \quad (15a)$$

$$\begin{aligned} \Delta G_{\text{red}}^{\text{Path2}} = & G_s(Mg) + G_{\text{THF}}(MgR1R2) - G_{\text{THF}}(MgR1^+) \\ & - G_{\text{THF}}(MgR2^+) - 2\Phi_M \end{aligned} \quad (15b)$$

$$\begin{aligned} \Delta G_{\text{red}}^{\text{Path3}} = & G_s(Mg) + G_{\text{THF}}(MgR1R2R3^-) - G_{\text{THF}}(MgR1^+) \\ & - G_{\text{THF}}(MgR2R3) - 2\Phi_M \end{aligned} \quad (15c)$$

where  $G_s(Mg)$  is the free energy of solid Mg,  $G_{\text{THF}}$  is the free energy of the complexes in THF, and  $\Phi_M$  is the work function of the inert metal electrodes. The influence of solvation on the reaction can be defined as the solvent reorganization energy ( $\lambda_{\text{solv}}$ )

$$\lambda_{\text{solv}}^{\text{Path1}} = \Delta G_{\text{THF}}(R1) - \Delta G_{\text{THF}}(MgR1^+) \quad (16a)$$

$$\lambda_{\text{solv}}^{\text{Path2}} = \Delta G_{\text{THF}}(MgR1R2) - \Delta G_{\text{THF}}(MgR1^+) - \Delta G_{\text{THF}}(MgR2^+) \quad (16b)$$

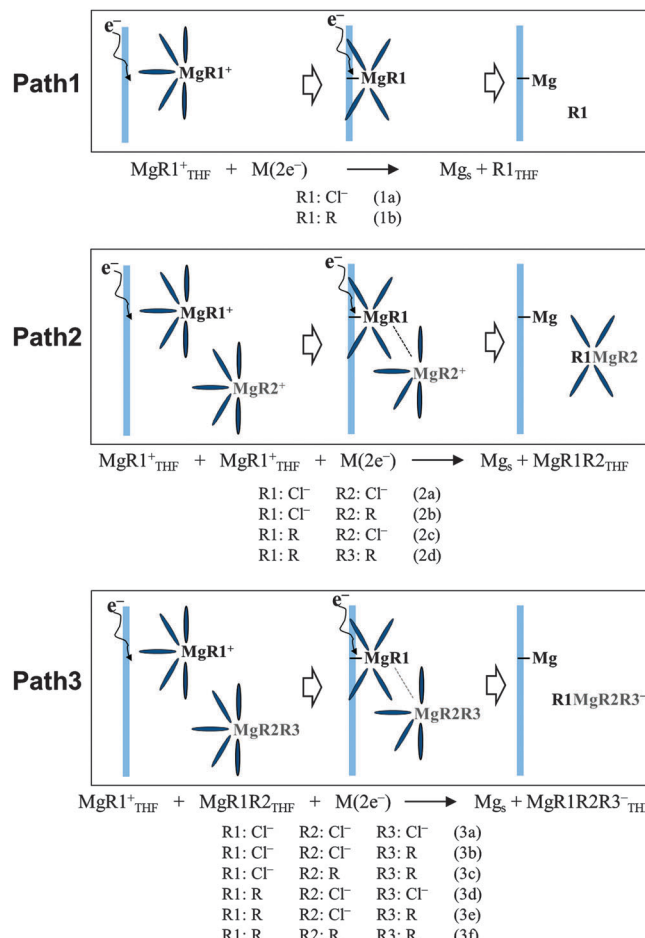


Fig. 6 Possible Mg-deposition pathways by double-electron transfer in  $RMgCl$ -based electrolytes.

$$\begin{aligned} \lambda_{\text{solv}}^{\text{Path3}} = & \Delta G_{\text{THF}}(MgR1R2R3^-) - \Delta G_{\text{THF}}(MgR1^+) \\ & - \Delta G_{\text{THF}}(MgR2R3) \end{aligned} \quad (16c)$$

The  $Mg/Mg^{2+}$  reduction potential in an aqueous medium ( $V_{\text{red,aq}}$ ) is  $-2.37$  V *versus* SHE (standard hydrogen electrode), *i.e.*,  $-4.14$  eV for two-electron reduction on the physical scale, and is given by

$$\Delta G_{\text{red,aq}} = G_s(Mg) - G_{\text{aq}}(Mg^{2+}) - 2\Phi_M \quad (17)$$

where  $G_{\text{aq}}(Mg^{2+})$  is the free energy of  $Mg^{2+}$  in the aqueous phase. The  $\Delta G_{\text{red}}$  values can then be expressed, by substituting eqn (16) and (17) into eqn (15), as

$$\Delta G_{\text{red}}^{\text{Path1}} = -4.14 + G_{\text{aq}}(Mg^{2+}) + G_g(R1) - G_g(MgR1^+) + \lambda_{\text{solv}}^{\text{Path1}} \quad (18a)$$

$$\begin{aligned} \Delta G_{\text{red}}^{\text{Path2}} = & -4.14 + G_{\text{aq}}(Mg^{2+}) + G_g(MgR1R2) - G_g(MgR1^+) \\ & - G_g(MgR2^+) + \lambda_{\text{solv}}^{\text{Path2}} \end{aligned} \quad (18b)$$

$$\begin{aligned} \Delta G_{\text{red}}^{\text{Path3}} = & -4.14 + G_{\text{aq}}(Mg^{2+}) + G_g(MgR1R2R3^-) - G_g(MgR1^+) \\ & - G_g(MgR2R3) + \lambda_{\text{solv}}^{\text{Path3}} \end{aligned} \quad (18c)$$

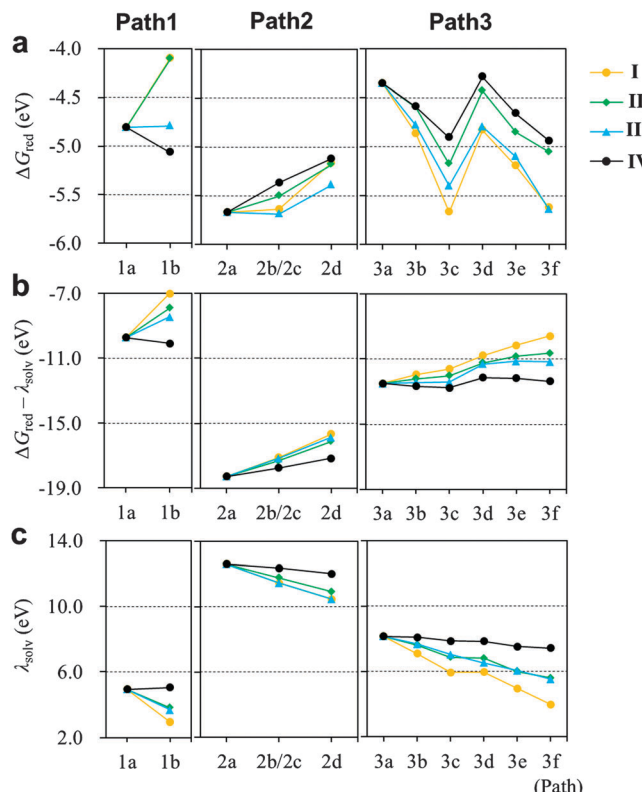


Fig. 7 Comparisons of reduction energies  $\Delta G_{\text{red}}$  (a),  $\Delta G_{\text{red}} - \lambda_{\text{solv}}$  (b), and solvent reorganization energies  $\lambda_{\text{solv}}$  (c) of Paths 1–3 for I–IV at the M062X/6-311+G\*\* level. Tables of energy values are available in the ESI† (SI-3).

where  $G_g$  is the free energy of the complexes in the gas phase. The  $\Delta G_{\text{red}}$  and  $\lambda_{\text{solv}}$  values for Paths 1–3 for I–IV are plotted in Fig. 7.

In the case of Path 1, as the bonding strength between Mg and R in the reactant complex  $\text{MgR}^+$  decreases,  $\Delta G_{\text{red}}$  decreases because of destabilization of the reactant. Fig. 7 shows that  $\Delta G_{\text{red}}$  for Path 1b for I/II is  $-4.1$  eV, and that for IV is  $-5.1$  eV. The  $\Delta G_{\text{red}}$  values for Path 2 are lower than those for Path 1, because of the formation of stable Mg complexes ( $\text{MgR}_1\text{R}_2$ ). Path 2a, in which Mg deposition occurs from  $\text{MgCl}^+$  with the aid of another  $\text{MgCl}^+$ , has the lowest reduction energy,  $-5.7$  eV. This is related to  $\Delta\Delta G_{\text{int}}$  ( $n = 2$ ) being lowest for  $\text{Cl}^-$  (Fig. 2a). In contrast to Path 1,  $\Delta G_{\text{red}}$  increases with increasing IE<sub>1</sub> of R in Path 2. Because two cationic complexes are involved in the Mg-deposition process, solvents stabilize the reaction more effectively. An increase in the IE<sub>1</sub> of R leads to increased solvation stabilization of the reactant, leading to an increase in  $\lambda_{\text{solv}}$ . In the case of Path 3, Path 3a, in which deposition occurs via  $\text{MgCl}^+$ , aided by  $\text{MgCl}_2$ , with formation of  $\text{MgCl}_3^-$ , has the highest reduction energy,  $-4.4$  eV. An increase in the IE<sub>1</sub> of R leads to an increase in  $\lambda_{\text{solv}}$ , as in Path 2, but weak solvation stabilization of the produced anion complexes leads to more clear changes in  $\lambda_{\text{solv}}$  with changes in the IE<sub>1</sub> of R.

The Mg-deposition process occurs by thermodynamics based on Mg-transfer kinetics. The contribution rate for each path was approximately calculated (Table 1) based on the ratios

Table 1 Reduction energies ( $\Delta G_{\text{red}}$ , eV) of Paths 1–3 for I–IV<sup>a</sup>

Path	I	II	III	IV
1a	<b>-4.81</b> (0.1)	<b>-4.81</b> (0.0)	<b>-4.81</b> (0.7)	<b>-4.81</b> (0.0)
1b	<b>-4.10</b> (0.9)	<b>-4.11</b> (1.0)	<b>-4.79</b> (0.3)	<b>-5.06</b> (1.0)
<b>1</b>	<b>-4.25</b>	<b>-4.11</b>	<b>-4.80</b>	<b>-5.06</b>
2a	<b>-5.67</b> (0.0)	<b>-5.67</b> (0.0)	<b>-5.67</b> (0.5)	<b>-5.67</b> (0.0)
2b	<b>-5.64</b> (0.2)	<b>-5.51</b> (0.0)	<b>-5.69</b> (0.4)	<b>-5.37</b> (0.0)
2d	<b>-5.17</b> (0.8)	<b>-5.18</b> (1.0)	<b>-5.39</b> (0.1)	<b>-5.12</b> (1.0)
<b>2</b>	<b>-5.35</b>	<b>-5.18</b>	<b>-5.65</b>	<b>-5.12</b>
3a	<b>-4.35</b> (0.0)	<b>-4.35</b> (0.0)	<b>-4.35</b> (0.4)	<b>-4.35</b> (0.0)
3b	<b>-4.86</b> (0.1)	<b>-4.60</b> (0.0)	<b>-4.78</b> (0.3)	<b>-4.59</b> (0.0)
3c	<b>-5.67</b> (0.0)	<b>-5.18</b> (0.0)	<b>-5.40</b> (0.0)	<b>-4.91</b> (0.0)
3d	<b>-4.83</b> (0.3)	<b>-4.43</b> (0.2)	<b>-4.80</b> (0.2)	<b>-4.29</b> (0.4)
3e	<b>-5.20</b> (0.6)	<b>-4.85</b> (0.8)	<b>-5.10</b> (0.1)	<b>-4.66</b> (0.2)
3f	<b>-5.62</b> (0.0)	<b>-5.06</b> (0.0)	<b>-5.64</b> (0.0)	<b>-4.94</b> (0.4)
<b>3</b>	<b>-5.00</b>	<b>-4.77</b>	<b>-4.69</b>	<b>-4.62</b>

<sup>a</sup> The data in parentheses are the contribution rates for each path, calculated based on the neutral- and cation-species ratios ( $\alpha$  and  $\beta$ ). The average reduction energies of each path are shown in bold characters.

of neutral and cationic species ( $\alpha$  and  $\beta$ ) from our modeling study of equilibria; the ion concentration gradient at the electrode–electrolyte interface was ignored. In the cases of I and II, which have covalent Mg–R bonds, and  $[\text{RMg}]^+$  is the dominant cationic species, the favored producing species for Mg deposition are Mg complexes (Paths 2d and 3d–e). The contribution of Path 3e is highest to Path 3, because  $\text{RMgCl}$  is the dominant neutral species for I and II. The average values of  $\Delta G_{\text{red}}$  in Path 3 for I and II are  $-5.0$  and  $-4.8$  eV, respectively; these values are  $0.7$  eV lower than those of Path 1. In the case of III, which causes steric hindrance, almost equal amounts of  $[\text{MgCl}]^+$  and  $[\text{RMg}]^+$  are present, but  $[\text{MgCl}]^+$  dominates slightly. For III, the average value of  $\Delta G_{\text{red}}$  for Path 1 is  $0.1$  eV lower than that for Path 3. At a high cation concentration at the electrode–electrolyte interface, the probability of Mg deposition *via* Path 2 would be increased. The average values of  $\Delta G_{\text{red}}$  *via* Path 2 are  $-5.4$ ,  $-5.2$ , and  $-5.7$  eV for I, II, and III, respectively (on the potential scale,  $-1.8$ ,  $-1.9$ , and  $-1.6$  V *versus* SHE, respectively). In the case of IV, which has a more ionic Mg–R bond, the favored producing species for Mg deposition is the monomeric anionic form of R (Path 1b). The  $\Delta G_{\text{red}}$  of Path 1 for IV is  $-5.1$  eV (on the potential scale,  $-1.9$  V *versus* SHE), which is almost isoenergetic with Path 2. The  $V_{\text{red}}$  of a  $\text{RMgCl}$  electrolyte in THF is therefore expected to be much higher than  $V_{\text{red},\text{aq}}$ . In the case of a Li electrode, the Li/Li<sup>+</sup> potential difference between aqueous and organic electrolytes depends only on variations in the solvation free energy of  $\text{Li}^+$ .<sup>31</sup> However, in the case of the Mg electrode, the Mg/Mg<sup>2+</sup> potential difference is determined by processes involving both salts and solvents.

#### 4. Electrochemical windows

Electrolyte oxidation involves loss of one electron from the highest occupied molecular orbital (HOMO) of anions or solvents in the electrolytes. The HOMO energies are highly correlated with the IE<sub>1</sub>.<sup>39–41</sup> The linear correlation between the HOMO energies and IE<sub>1</sub> values of selected molecules is presented in Fig. 8a. The HOMO energy levels of anionic Mg complexes  $[\text{R}_n\text{MgCl}_m]^-$  change

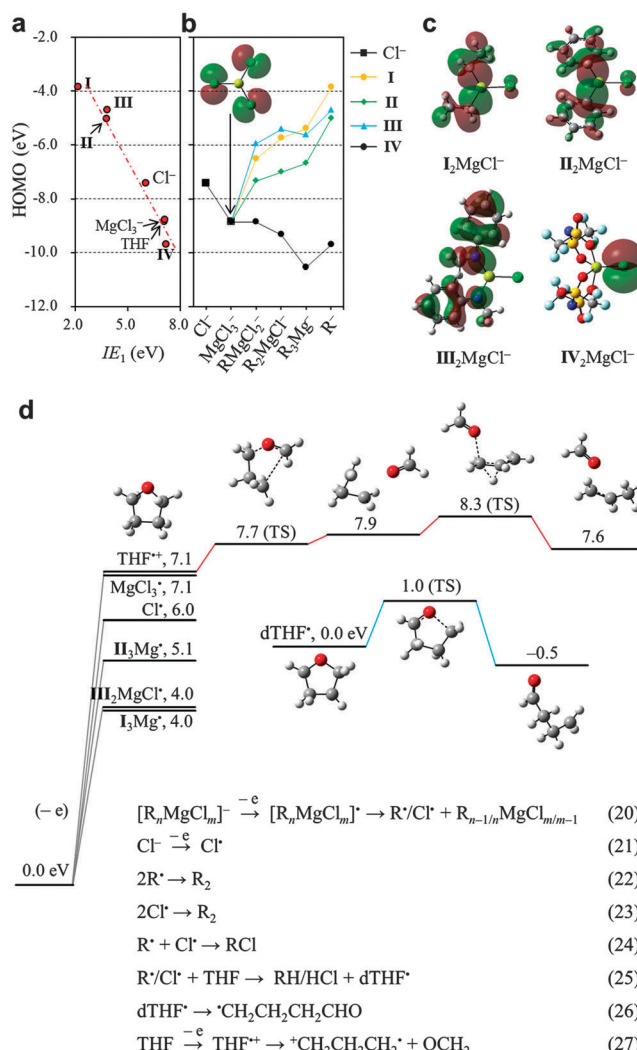


**Fig. 8** (a) Linear relationship between HOMO energies at the M062X/6-311+G\*\* level and  $\text{IE}_1$  values at the CCSD(T)/aug-cc-pVDZ level in the THF phase ( $\text{IE}_1 = -0.85 \times \text{HOMO} - 0.57$ ). (b) Changing trends in the HOMO energy levels of  $[\text{R}_n\text{MgCl}_m]^-$  depending on the R and  $n:m$  ratio. Representative HOMOs of  $[\text{MgCl}_3]^-$  (b, inset) and  $[\text{R}_2\text{MgCl}]^-$  for I–IV (c). (d)  $\text{IE}_1$  values of components most susceptible to oxidation for I–IV and oxidative degradation mechanisms (eqn (20)–(27)). THF degradation pathways are investigated at the CCSD(T)/aug-cc-pVDZ level.

depending on the  $n:m$  ratio and the characteristics of R (Fig. 8b). When the HOMO energy of  $\text{Cl}^-$  is higher than that of R, as in the case of **IV**, the HOMO energy of  $[\text{R}_n\text{MgCl}_m]^-$  decreases with increasing  $n$ . The HOMO energies of  $[\text{MgCl}_3]^-$ ,  $[\text{IV}_2\text{MgCl}]^-$ ,  $[\text{IV}_3\text{Mg}]^-$ , and  $[\text{IV}_n\text{MgCl}_m]^-$  are  $-8.9$ ,  $-8.9$ ,  $-9.4$ , and  $-10.6$  eV, respectively. However, when the HOMO energy of R is higher than that of  $\text{Cl}^-$ , as in the cases of **I** and **II**, the HOMOs of  $[\text{I}_n/\text{II}_n\text{MgCl}_m]^-$  are localized on the  $\sigma$ -bonding orbital of **I**/**II**–Mg (Fig. 8c), so the HOMO energies of  $[\text{I}_n/\text{II}_n\text{MgCl}_m]^-$  increase with increasing  $n$ . The HOMO energies of  $[\text{IMgCl}_2]^-$ ,  $[\text{I}_2\text{MgCl}]^-$ , and  $[\text{I}_3\text{Mg}]^-$  are  $-6.5$ ,  $-5.8$ , and  $-5.4$  eV, respectively; the HOMO energies of  $[\text{IIIMgCl}_2]^-$ ,  $[\text{II}_2\text{MgCl}]^-$ , and  $[\text{II}_3\text{Mg}]^-$  are  $-7.4$ ,  $-7.0$ , and  $-6.7$  eV, respectively. In the case of **III**, the HOMO of  $[\text{III}_n\text{MgCl}_m]^-$  is localized on the non-bonding  $p_z$  orbital of **III**, and

**Table 2** HOMO energies and  $\text{IE}_1$  values of anions for I–IV (eV)<sup>a</sup>

Path	I	II	III	IV
$\text{Cl}^-$	$-7.44$ (6.03)	$-7.44$ (6.03)	$-7.44$ (6.03)	$-7.44$ (6.03)
$\text{MgCl}_3^-$	$-8.87$ (7.07)	$-8.87$ (7.07)	$-8.87$ (7.07)	$-8.87$ (7.07)
$\text{RMgCl}_2^-$	$-6.51$ (4.96)	$-7.35$ (5.67)	$-5.95$ (4.48)	$-8.86$ (6.95)
$\text{R}_2\text{MgCl}^-$	$-5.75$ (4.31)	$-7.01$ (5.37)	$-5.41$ (4.02)	$-9.35$ (7.36)
$\text{R}_3\text{Mg}^-$	$-5.39$ (4.00)	$-6.69$ (5.11)	$-5.64$ (4.21)	$-10.55$ (8.38)
R <sup>-</sup>	$-3.86$ (2.15)	$-5.03$ (3.79)	$-4.71$ (3.80)	$-9.71$ (7.17)

<sup>a</sup>  $\text{IE}_1$  values are in parentheses; those in italic characters are values calculated at the CCSD(T)/aug-cc-pVDZ level; the others are fitting values from the linear relationships between the HOMO energies at the M062X/6-311+G\*\* level and calculated  $\text{IE}_1$  values.

the HOMO energy of  $[\text{III}_2\text{MgCl}]^-$  ( $-5.4$  eV) is higher than that of  $[\text{III}_3\text{Mg}]^-$  ( $-5.6$  eV). Although the HOMO energy of R for **III** is very similar to that for **II**, the HOMO energies of anionic **III**–Mg complexes are more than  $\sim 1$  eV higher than those of **II**–Mg complexes, because of steric hindrance by **III**. This results in lowering of the oxidation potential of **III** compared with that of **II**. In Table 2, the  $\text{IE}_1$  values of  $[\text{R}_n\text{MgCl}_m]^-$  are evaluated from the linear relationship between the HOMO energies and the calculated  $\text{IE}_1$  values.

The components most susceptible to oxidation in the electrolytes are  $[\text{R}_3\text{Mg}]^-$  for **I** and **II**, and  $[\text{R}_2\text{MgCl}]^-$  for **III**. The  $\text{IE}_1$  values of  $[\text{I}_3\text{Mg}]^-$ ,  $[\text{II}_3\text{Mg}]^-$ , and  $[\text{III}_2\text{MgCl}]^-$  are  $4.0$ ,  $5.1$ , and  $4.0$  eV, respectively (Table 2). Although the monomeric anion R has the highest HOMO for **I**–**III**, it rarely exists, because of the molar ratios of the anions,  $\gamma$  (ratio of R/ $[\text{R}_3\text{Mg}]^- < 10^{-17}$ ). However, the amounts of  $[\text{MgCl}_3]^-$  and monomeric anions of R and  $\text{Cl}^-$  are higher for **IV**, and  $\text{Cl}^-$  becomes the component most susceptible to oxidation for **IV**. The  $\text{IE}_1$  of  $\text{Cl}^-$  is  $6.0$  eV. The oxidation potentials versus  $\text{Mg/Mg}^{2+}$  ( $V_{\text{ox vs. Mg}}$ ) are calculated from

$$V_{\text{ox vs. Mg}} = (\text{IE}_1 + \Delta G_{\text{red}}/2)/F \quad (19)$$

where  $F$  is the Faraday constant ( $1 \text{ eV V}^{-1}$ ). Based on the average values of  $\Delta G_{\text{red}}^{\text{Path}2}$ , the predicted  $V_{\text{ox vs. Mg}}$  values are  $1.4$ ,  $2.5$ ,  $1.2$ , and  $3.5$  V for **I**, **II**, **III**, and **IV**, respectively; these are in good agreement with the experimental values. It should be noted that the experimental oxidation potentials are thermodynamic potentials based on kinetic measurements, and the electrode surface plays a catalytic role in electrolyte oxidation.<sup>42</sup>

We also predicted the electrochemical window of HMDSMgCl in THF. The HOMO energy of the HMDS anion, which has an electron-rich Si–N–Si core, is  $-6.1$  eV, which is  $1.4$  eV lower than that of **II**. However, the steric hindrance of HMDS leads to less stable HMDS–Mg complexation; therefore, although the HOMO energy of the HMDS anion is lower than that of **II**, the HOMO energies of anionic HMDS–Mg complexes are slightly higher than those of **II**–Mg complexes. The HOMO energy values of  $[\text{HMDSMgCl}_2]^-$ ,  $[\text{HMDS}_2\text{MgCl}]^-$ , and  $[\text{HMDS}_3\text{Mg}]^-$  are  $-6.9$ ,  $-6.8$ , and  $-6.5$  eV, respectively (Fig. 9). From the linear relationship between the HOMO energies and  $\text{IE}_1$  values, the  $\text{IE}_1$  of  $[\text{HMDS}_3\text{Mg}]^-$ , which is the component most susceptible to oxidation in HMDSMgCl electrolytes, is  $5.0$  eV. The  $V_{\text{ox vs. Mg}}$  of HMDSMgCl in THF is approximately predicted to be  $2.2$  V, based on  $\Delta G_{\text{red}}^{\text{Path}2a}$ , which is in good agreement with the experimental data.<sup>13</sup>

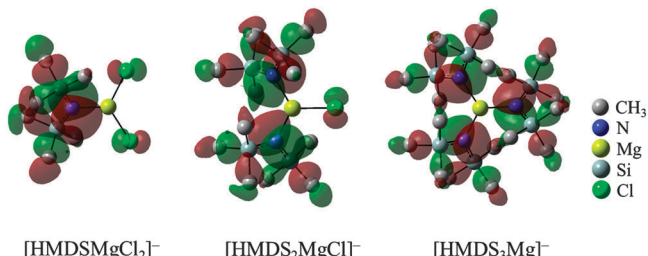


Fig. 9 Representative HOMOs of  $[\text{HMDSMgCl}_2]^-$ ,  $[\text{HMDS}_2\text{MgCl}]^-$ , and  $[\text{HMDS}_3\text{Mg}]^-$ .

Oxidation of  $[\text{R}_n\text{MgCl}_m]^-$  or  $\text{Cl}^-$  forms  $\text{R}^\bullet$  or  $\text{Cl}^\bullet$  radicals (eqn (20) and (21)), which immediately undergo coupling (eqn (22)–(24)) or other reactions.  $\text{R}^\bullet/\text{Cl}^\bullet$  can react with THF, producing  $\text{RH}/\text{HCl}$ ,<sup>20</sup> and a deprotonated THF radical ( $\text{dTHF}^\bullet$ ) (eqn (25));  $\text{dTHF}^\bullet$  and ring-opened  $\text{dTHF}^\bullet$ , which has a formation activation barrier of 1 eV (eqn (26)), also immediately undergo other reactions.<sup>43</sup> The  $\text{IE}_1$  of THF is 7.1 eV, which is almost isoenergetic with that of  $[\text{MgCl}_3]^-$ . The  $V_{\text{ox}}$  of THF is therefore higher than those of the species most susceptible to oxidation for **I**–**IV**:  $[\text{R}_3\text{MgCl}]^-$  for **I** and **II**,  $[\text{R}_2\text{MgCl}]^-$  for **III**, and  $\text{Cl}^-$  for **IV**. Oxidation of a THF solvent molecule produces a (cyclo)propane radical cation and formaldehyde (eqn (27)).<sup>44</sup>

## 5. Conclusions

In summary, the equilibrium of  $\text{RMgCl}$  in THF is complex with a mixture of various combinations of compounds, determined by the characteristics of R groups. As the first ionization energy of R increases, the strength of the Mg–R bond becomes unstable. It leads to increases of the solvation stabilization of Mg–R complexes, resulting in increases of the relative dominance of a neutral  $\text{R}_2\text{Mg}$  species, an  $[\text{MgR}]^+$  cation, and monomeric R and  $\text{Cl}^-$  anions. While the dominant neutral species is  $\text{RMgCl}$  with a covalent R–Mg bond, the dominance of  $\text{R}_2\text{Mg}$  increases with increasing ionic nature of the R–Mg bond. As the source of  $\text{MgCl}_2$  is not only the Schlenk equilibrium but also the formation of R-involving ionic species, the molar ratio of  $[\text{MgCl}_2]/[\text{R}_2\text{Mg}]$  is usually more than 1. Whereas, steric hindrance of R destabilizes Mg complexation, resulting in a decrease of the relative dominance of  $\text{R}_2\text{Mg}$  and  $[\text{RMg}]^+$ . In the Mg-reduction processes, the producing species, which favor Mg complexes with covalent Mg–R bonds, become monomeric anions with increasing ionic nature of the Mg–R bond. The Mg-reduction potential values in  $\text{RMgCl}$ -electrolytes are expected to be almost 0.5 V higher than that in the aqueous phase by calculation. The Mg reduction potential can be controlled by stabilizing the reactant or destabilizing the product in the Mg-deposition process. In the electrolyte-oxidation processes, the most susceptible components to oxidation are anionic Mg complexes with a covalent R–Mg bond. The steric hindrance of R leads to destabilization of anionic Mg complexes with a lowered width of an electrochemical window. However, the relative dominances of monomeric anions of R and  $\text{Cl}^-$  increase with increasing ionic nature of R–Mg; and

monomeric anions become the most susceptible component to oxidation.

One of the most important issues in the development of  $\text{RMgCl}$  electrolytes is electrochemical windows. We predict that the maximum potential range between Mg deposition and the irreversible oxidation of the electrolyte gives a window of electrochemical stability of almost 3.5 V when  $\text{Cl}^-$  becomes the component most susceptible to oxidation in a system such as **IV**. However, the delocalized electrons of **IV** have an increased tendency toward reduction; therefore, **IV** is not compatible with a Mg anode forming a passivating surface.<sup>45</sup> The S–CF<sub>3</sub> bond in **IV** would be broken on the Mg surface, forming Mg–F and Mg–CF<sub>2</sub>, in the initial step (SI-4, ESI†). Thus, to maximize the electrochemical windows and oxidative and reductive stabilities, R should be selected based on the following criteria: the  $\text{IE}_1$  values of the anionic Mg complexes  $[\text{R}_n\text{MgCl}_m]^-$  should be lower than that of  $\text{Cl}^-$ , and R should be inert to the anode and cathode surfaces. We also note that the air/moisture sensitivity of  $\text{RMgCl}$  usually decreases with increasing ionic character of the R–Mg bond (ESI-5†). However,  $\text{RMgCl}$  electrolytes in complex chemical equilibria have multiple pathways for Mg/electrolyte reduction/oxidation processes, which make the process difficult to control, justifying the development of simpler electrolytes.

To increase the oxidation stability and conductivity, electrolyte solutions based on the reaction of  $\text{RMgCl}$  with Lewis acid complexes have been investigated. For example, electrolyte solutions of  $\text{PhMgCl}/\text{HMDSMgCl}$  reacting with  $\text{AlCl}_3$  in the optimal ratio show an electrochemical window of ~3.2 V.<sup>19,20,46</sup> Transmetalation of R from Mg to Al changes the species that is most susceptible to oxidation from anionic Mg complexes  $[\text{R}_3\text{Mg}]^-$  to anionic Al complexes  $[\text{R}_4\text{Al}]^-$ .<sup>47</sup> The HOMO energy of  $[\text{Ph}_4\text{Al}]^-$  is −7.2 eV in THF, and the  $\text{IE}_1$  is calculated to be ~5.6 in THF, which is more than 0.5 eV higher than the  $\text{IE}_1$  of  $[\text{Ph}_3\text{Mg}]^-$ . However, since  $\text{Cl}^-$  gives the upper limit of the electrochemical window, R should be selected such that the  $\text{IE}_1$  values of anionic Al complexes  $[\text{R}_n\text{AlCl}_m]^-$  are lower than that of  $\text{Cl}^-$ , to maximize the electrochemical window. We are currently screening R groups to identify the optimal groups for Mg electrolytes, using a combined theoretical and experimental approach. Recently, there have been attempts to develop non-halogen-containing electrolytes,<sup>21,22,48</sup> because halogen-containing electrolytes corrode the conventional metal current collectors.<sup>5</sup> We believe that the design of receptors and host-guest chemistry based on molecular information<sup>49–51</sup> will be very useful for further development of novel Mg electrolytes.

Our molecular model study identified important rules and trends related to the characteristics of Mg complexes, solvation, chemical equilibria, and the processes of Mg deposition, electrolyte oxidation, and degradation of  $\text{RMgCl}$ -based electrolytes. We have provided a methodological scheme for calculating Mg reduction potentials in non-aqueous electrolytes and electrochemical windows between Mg deposition and electrolyte oxidation. This study therefore provides a strategy for designing Mg electrolytes to maximize their reductive and oxidative stabilities and electrochemical windows. This study is highly

beneficial not only for the design of improved Mg electrolytes, but also for the future development of new electrolytes for advanced energy-storage applications.<sup>52</sup>

## Acknowledgements

The authors thank all the members of the Non-Li Battery Project at SAIT for useful comments and discussion.

## References

- M. Armand and J.-M. Tarascon, *Nature*, 2008, **451**, 652–657.
- B. Dunn, H. Kamath and J.-M. Tarascon, *Science*, 2011, **334**, 928–935.
- D. Aurbach, Z. Lu, A. Schechter, Y. Gofer, H. Gizbar, R. Turgeman, Y. Cohen, M. Moshkovich and E. Levi, *Nature*, 2000, **407**, 724–727.
- J. O. Besenhard and M. Winter, *ChemPhysChem*, 2002, **3**, 155–159.
- H. D. Yoo, I. Shterenberg, Y. Gofer, G. Gershinsky, N. Pour and D. Aurbach, *Energy Environ. Sci.*, 2013, **6**, 2265–2279.
- C. Ling, D. Banerjee and M. Matsui, *Electrochim. Acta*, 2012, **76**, 270–274.
- K. Xu, *Chem. Rev.*, 2004, **104**, 4303–4417.
- Z. Lu, A. Schechter, M. Moshkovich and D. Aurbach, *J. Electroanal. Chem.*, 1999, **466**, 203–217.
- D. Seyferth, *Organometallics*, 2009, **28**, 1598–1605.
- I. W. Gaddum and H. E. French, *J. Am. Chem. Soc.*, 1927, **49**, 1295–1299.
- W. V. Evans and R. Pearson, *J. Am. Chem. Soc.*, 1942, **64**, 2865–2871.
- T. D. Gregory, R. J. Hoffman and R. C. Winterton, *J. Electrochem. Soc.*, 1990, **137**, 775–780.
- C. Liebenow, Z. Yang and P. Lobitz, *Electrochim. Commun.*, 2000, **2**, 641–645.
- D. Aurbach, M. Moshkovich, A. Schechter and R. Turgeman, *Electrochim. Solid-State Lett.*, 2000, **3**, 31–34.
- D. Aurbach, R. Turgeman, O. Chusid and Y. Gofer, *Electrochim. Commun.*, 2001, **3**, 252–261.
- D. Aurbach, A. Schechter, M. Moshkovich and Y. Cohen, *J. Electrochem. Soc.*, 2001, **148**, A1004–A1014.
- D. Aurbach, H. Gizbar, A. Schechter, O. Chusid, H. E. Gottlieb, Y. Gofer and I. Goldberg, *J. Electrochem. Soc.*, 2002, **149**, A115–A121.
- Y. Vestfried, O. Chusid, Y. Goffer, P. Aped and D. Aurbach, *Organometallics*, 2007, **26**, 3130–3137.
- O. Mizrahi, N. Amir, E. Pollak, O. Chusid, V. Marks, H. Gottlieb, L. Larush, E. Zinigrad and D. Aurbach, *J. Electrochem. Soc.*, 2008, **155**, A103–A109.
- H. S. Kim, T. S. Arthur, G. D. Allred, J. Zajicek, J. G. Newman, A. E. Rodnyansky, A. G. Oliver, W. C. Boggess and J. Muldoon, *Nat. Commun.*, 2011, **2**, 427–432.
- J. Muldoon, C. B. Bucur, A. G. Oliver, J. Zajicek, G. D. Allred and W. C. Boggess, *Energy Environ. Sci.*, 2013, **6**, 482–487.
- J. Zhu, Y. Guo, J. Yang, Y. Nuli, F. Zhang, J. Wang and S.-I. Hirano, *J. Power Sources*, 2014, **248**, 690–694.
- O. Malyi, V. V. Kulish, T. L. Tan and S. Manzhos, *Nano Energy*, 2013, **2**, 1149–1157.
- Y. Shao, M. Gu, X. Li, Z. Nie, P. Zuo, G. Li, T. Liu, J. Xiao, Y. Cheng, C. Wang, J.-G. Zhang and J. Liu, *Nano Lett.*, 2014, **14**, 255–260.
- O. Malyi, T. L. Tan and S. Manzhos, *J. Power Sources*, 2013, **233**, 341–345.
- N. Singh, T. S. Arthur, C. Ling, M. Matsui and F. Mizuno, *Chem. Commun.*, 2013, **49**, 149–151.
- Z. Wang, Q. Su, J. Shi, H. Deng, G. Q. Yin, J. Guan, M. P. Wu, Y. L. Zhou, H. L. Lou and Y. Q. Fu, *ACS Appl. Mater. Interfaces*, 2014, **6**, 6786–6789.
- D. Y. Kim, H. M. Lee, S. K. Min, Y. Cho, I.-C. Hwang, K. Han, J. Y. Kim and K. S. Kim, *J. Phys. Chem. Lett.*, 2011, **2**, 689–694.
- D. Y. Kim, H. M. Lee, J. Seo, S. K. Shin and K. S. Kim, *Phys. Chem. Chem. Phys.*, 2010, **12**, 5446–5453.
- D. Y. Kim, N. J. Singh, H. M. Lee and K. S. Kim, *Chem. – Eur. J.*, 2009, **15**, 5598–5604.
- Y. Wang, S. Nakamura, M. Ue and P. B. Balbuena, *J. Am. Chem. Soc.*, 2001, **123**, 11708–11718.
- J. Yu, P. B. Balbuena, J. Budzien and K. Leung, *J. Electrochem. Soc.*, 2011, **158**, A400–A410.
- R. Arnaud, D. Benrabah and J.-Y. Sanchez, *J. Phys. Chem.*, 1996, **100**, 10882–10891.
- V. Aravindan, J. Gnanaraj, S. Madhavi and H.-K. Liu, *Chem. – Eur. J.*, 2011, **17**, 14326–14346.
- M. J. Frisch, G. W. Trucks, H. B. Schlegel, G. E. Scuseria, M. A. Robb, J. R. Cheeseman, G. Scalmani, V. Barone, B. Mennucci, G. A. Petersson, H. Nakatsuji, M. Caricato, X. Li, H. P. Hratchian, A. F. Izmaylov, J. Bloino, G. Zheng, J. L. Sonnenberg, M. Hada, M. Ehara, K. Toyota, R. Fukuda, J. Hasegawa, M. Ishida, T. Nakajima, Y. Honda, O. Kitao, H. Nakai, T. Vreven, J. A. Montgomery, Jr., J. E. Peralta, F. Ogliaro, M. Bearpark, J. J. Heyd, E. Brothers, K. N. Kudin, V. N. Staroverov, R. Kobayashi, J. Normand, K. Raghavachari, A. Rendell, J. C. Burant, S. S. Iyengar, J. Tomasi, M. Cossi, N. Rega, J. M. Millam, M. Klene, J. E. Knox, J. B. Cross, V. Bakken, C. Adamo, J. Jaramillo, R. Gomperts, R. E. Stratmann, O. Yazyev, A. J. Austin, R. Cammi, C. Pomelli, J. W. Ochterski, R. L. Martin, K. Morokuma, V. G. Zakrzewski, G. A. Voth, P. Salvador, J. J. Dannenberg, S. Dapprich, A. D. Daniels, Ö. Farkas, J. B. Foresman, J. V. Ortiz, J. Cioslowski and D. J. Fox, *Gaussian 09, Revision D.01*, Gaussian, Inc., Wallingford, CT, USA, 2009.
- R. J. Bartlett and G. D. Purvis III, *Int. J. Quantum Chem.*, 1978, **14**, 561–581.
- G. E. Parris and E. C. Ashby, *J. Am. Chem. Soc.*, 1971, **93**, 1206–1213.
- Y. Zhao and D. G. Truhlar, *Theor. Chem. Acc.*, 2008, **120**, 215–241.
- N. Shao, X.-G. Sun, S. Dai and D.-E. Jiang, *J. Phys. Chem. B*, 2011, **115**, 12120–12125.
- S. P. Ong and G. Ceder, *Electrochim. Acta*, 2010, **55**, 3804–3811.

- 41 V. D. Parker, *J. Am. Chem. Soc.*, 1976, **98**, 98–103.
- 42 K. Leung, *J. Phys. Chem. C*, 2012, **116**, 9852–9861.
- 43 T. Fuchigami, T. Sato and T. Nonaka, *J. Org. Chem.*, 1986, **51**, 366–369.
- 44 X. Zhang, J. K. Pugh and P. N. Ross, *J. Electrochem. Soc.*, 2001, **148**, E183–E188.
- 45 H. S. Kim, J. Muldoon and M. Matsui, 217th ECS Meeting, Abstract 225.
- 46 J. Muldoon, C. B. Bucur, A. G. Oliver, T. Sugimoto, M. Matsui, H. S. Kim, G. D. Allred, J. Zajicek and Y. Kotani, *Energy Environ. Sci.*, 2012, **5**, 5941–5950.
- 47 N. Pour, Y. Gofer, D. T. Major and D. Aurbach, *J. Am. Chem. Soc.*, 2011, **133**, 6270–6278.
- 48 Y.-S. Guo, F. Zhang, J. Yang, F.-F. Wang, Y. NuLi and S.-I. Hirano, *Energy Environ. Sci.*, 2012, **5**, 9100–9106.
- 49 D. Y. Kim, N. J. Singh, J. W. Lee and K. S. Kim, *J. Chem. Theory Comput.*, 2008, **4**, 1162–1169.
- 50 D. Y. Kim, N. J. Singh and K. S. Kim, *J. Chem. Theory Comput.*, 2008, **4**, 1401–1407.
- 51 D. Y. Kim, I. Geronimo, N. J. Singh, H. M. Lee and K. S. Kim, *J. Chem. Theory Comput.*, 2012, **8**, 274–280.
- 52 K. Xu, *Energies*, 2010, **3**, 135–154.